Supplementary Information for

Late Permian core-surface-magnetosphere conditions revealed by single crystal paleointensities from the Emeishan large igneous province

Wentao Huang[1]*, John A. Tarduno[2,3], Zhenyu Yang[4], Richard K. Bono[5], Wenbin Tang[6], Yuntao Tian[7,8], Yong Yao[1], Zhenni Yi[1], Yahui Yue[1], Lin Ding[1]

[1]State Key Laboratory of Tibetan Plateau Earth System, Environment and Resources (TPESER), Institute of Tibetan Plateau Research, Chinese Academy of Sciences, Beijing 100101, China. *Corresponding author. Email: whuang@itpcas.ac.cn

[2]Department of Earth and Environmental Sciences, University of Rochester, Rochester, NY 14627, USA

[3]Department of Physics and Astronomy, University of Rochester, Rochester, NY 14627, USA

[4]College of Resources, Environment and Tourism, Capital Normal University, Beijing 100048, China

[5]Department of Earth, Ocean and Atmospheric Science, Florida State University, Tallahassee, FL 32306, USA,

[6]State Key Laboratory of Oil and Gas Reservoir Geology and Exploitation, Institute of Sedimentary Geology, Chengdu University of Technology, Chengdu 610059, China

[7]Guangdong Provincial Key Laboratory of Geodynamics and Geohazards, School of Earth Sciences and Engineering, Sun Yat-sen University, Zhuhai, 510275, China

[8]Southern Marine Science and Engineering Guangdong Laboratory, Zhuhai, 519082, China

This file includes:

Supplementary Texts 1 to 4

Supplementary Figures 1 to 12.

Supplementary Text 1: Geology of the Emeishan large igneous province

The Emeishan large igneous province (ELIP), derived from upwellings of a mantle plume[1,2], is located in the western Yangtze Block (Supplementary Fig. 1a). The province covers an area of >

2.5 x 10^5 km^2 with a variable thickness of a few hundred meters to ~5 km, and mainly consists of large volume of continental flood basalt and associated mafic-ultramafic intrusions[3,4]. In the Panzhihua region of the ELIP, a 300 km long by 10-30 km wide mineralized zone, composed of basalt, mafic-ultramafic intrusions, syenitic/granitic intrusions, and associated Fe-Ti-V oxide deposits, outcrops near Panzhihua, Hongge and Baima (Supplementary Fig. 1b). Sedimentologic and biostratigraphic evidence constrain formation of the ELIP to the Late Permian[5-7]. Zircon U-Pb chemical-abrasion thermal ionization mass spectrometry (CA-TIMS) geochronology with superior precision yielded tightly clustered ages between 257.22 ± 0.37 Ma and 260.55 ± 0.07 Ma for the extrusive and intrusive rocks of the ELIP[8-10], which concurs with the rapid emplacement of the ELIP with a short duration of ~2 Myr indicated by magnetostratigraphic and sedimentologic studies[6,11-13]. Recent $^{40}Ar/^{30}Ar$ dating on fresh plagioclase grains from the ELIP basalt yielded a mean age of 260.1 ± 1.2 Ma from five measurements[14], which is indistinguishable from the zircon CA-TIMS U-Pb dates of ignimbrite above the basalt[9]. These dates explain the younger whole rock $^{40}Ar/^{30}Ar$ ages (251 - 256 Ma) in previously studies[15,16] as due to unrecognized partial loss of radiogenic argon, and that the ELIP did not experience thermal resetting induced by regional tectonic activities soon after emplacement[14,17].

In the Baima area of the Panzhihua region, N-S striking intrusions of the ELIP are well exposed with the mafic-ultramafic intrusions surrounded by coeval syenitic and granitic intrusions (Supplementary Fig. 1b-f). These intrusions intruded the Precambrian strata and were cut by several faults striking NE-SW. The mafic-ultramafic intrusions are ~20 km long and 1-4 km wide[18]. They show rhythmic layering of dark/light minerals and their grain size on centimeter-scale (Supplementary Fig. d), and were divided into the Fe-Ti-V oxide-mineralized Lower Zone and apatite-bearing Upper Zone[19]. The Lower Zone is dominated by thick medium-grained oxide ore intergrown with thick barren troctolite, but a few interlayers of olivine gabbro can also be observed. The Upper Zone is mainly composed of barren troctolite and olivine gabbro. Zircon U-Pb CA-TIMS dating investigations were conducted on six intrusive samples of mafic dyke, syenite, and granite near the Baima area[8]; these geochronologic samples are located 3.6-14.5 km away from our granite and gabbro sampling locality. The individual zircon ages yield a weighted mean age of 259.04 ± 0.25 Ma (Supplementary Fig. 2).

Regional studies at Panzhihua and Baima suggests the area has not seen pervasive metamorphic conditions exceeding 230 °C. Thermochronologic studies of the Neoproterozoic granites and Triassic sandstones (60-80 km away from our sampling locality) cooled down to 120 °C (closure temperature of apatite fission track) by ~37 Ma[20,21]. At the same time, the zircon fission track dates of Jurassic sandstones deposited above the ELIP (175 km northeast of our sampling locality) have been only partially reset, indicating that post-Jurassic heating of the rocks in this region did not exceed the closure temperature of the zircon fission track (230 °C)[22].

Supplementary Text 2: Prior paleomagnetic and paleointensity investigations of the ELIP

Prior paleomagnetic studies on the ELIP mostly focus on the extrusive flood basalt for magnetostratigraphy, tectonic reconstruction, and paleointensity[11-13,23-29]. Gabbro samples (one site, 8 samples) from the Upper Zone of the layered mafic intrusion in the Panzhihua area (26.81°N, 101.79°E, 40 km southwest of our sampling locality) were also investigated[30]. The reported paleomagnetic directional data vary in quality and quantity with the number of investigated lava flows ranging from only a few to >100 sites. Most of these results yield a near-equatorial paleolatitudes for the emplacement of the ELIP. For example, a large, robust paleomagnetic data set in the Binchuan area (25.85°N, 100.39°E) suggests an average characteristic remanent magnetization (ChRM) direction of declination/inclination = 74.0°/-9.6° from 99 lava sites[11], corresponding to a pole of 12.19°N/201.96E°, after converting all site-mean directions with reversed polarity to normal polarity and applying a 45° cutoff (Supplementary Fig. 3a, b). In contrast, the Xiongjiachang section of the southern ELIP exposed in the Zhijin area (26.48°N, 105.69°E), which was also studied for paleointensity[26], contains only 7 sites with scattered site-mean ChRM directions and yields an average direction of declination/inclination = 69.8°/33.1° (Supplementary Fig. 3c). The significant difference between the two average ChRM directions strongly suggests that magnetic records of the ELIP lavas in the Zhijin area are not robust; possible reasons include unaveraged secular variation and/or remagnetization. Remagnetization of the ELIP basalt related to late hydrothermal fluid circulation has been identified in a few localities[25,31].

The earliest published ELIP paleointensity results are from the basaltic lava flows in the Zhijin area (26.48°N, 105.69°E)[26], which were assigned an age of ~262 Ma by biostratigraphic dating of the interbedded and underlying limestones[7]. Rock magnetic experiments indicate multidomain

(MD) and single domain (SD) magnetite as the dominant magnetic carrier with maghemitization of magnetite observed in two units. Arai plots of the paleointensity data rarely show convex-down behavior, and the temperature range used for paleointensity calculation varies from 200 to 530 °C. A total of five lava flows yield site-mean paleointensity values of 14.2 - 35.3 μT with an average of 22.9 ± 7.7 μT, corresponding to a VDM of 5.9 ± 2.0 x 10^{22} A m^2 if the robust Binchuan pole is used to calculate the paleolatitude (0.08°S). The large dispersion of the ChRM directions, their significant deviation from other robust paleomagnetic directional results of the ELIP, the presence of nonideal magnetic minerology including MD magnetite and maghemite, and small number of the investigated fast cooling basaltic lava flows, considered in aggregate, casts doubt on the reliability of these paleointensity results. Preliminary paleointensities of ~10-20 μT from the ELIP basalt in other sections have been reported in a conference abstract[32], but the data are not published.

Recent bulk rock paleointensity studies of the ELIP were conducted on six lava flow sites from the Binchuan area (25.85°N, 100.39°E) and four lava flow sites from the Dongchuan (26.08°N, 103.05°E) area[33]. The average site-mean ChRM directions derived from these relatively small Binchuan and Dongchuan datasets differ from one another, and both differ from the mean ChRM defined by 99 lava flow sites from the Binchuan area[11] (Supplementary Fig. 3b, e, f), most likely reflecting geomagnetic secular variation and/or local vertical-axis rotation. The former is particularly important, as it suggests that these relatively small data may not adequately average geomagnetic secular variation. Rock magnetic tests of these lava flows indicate that the magnetic carriers are SD-MD low-Ti magnetite and hematite. Most samples meeting paleointensity data selection criteria used by the authors have double-slope Aria plots (some of which are concave upward indicating the presence of MD grains), and the high temperature segments between 450-705 °C are usually used to calculate the paleointensity value. These results yield site-mean values of 1.6-7.7 μT from the Binchuan lava units and 1.7-12.9 μT from the Dongchuan lava units. An average paleointensity of 4.9 ± 3.4 μT and a corresponding VDM of 1.3 ± 0.9 x 10^{22} A m^2 are determined from the overall 10 lava units[33]. However, we note that the contribution of hematite to the remanence used to define the whole rock paleointensity questions the accuracy of the reported values. Based on the identification of hematite through a maximum unblocking temperature exceeding 580 °C (i.e., the Curie temperature of magnetite) and hysteresis parameters, this hematite contribution is significant or dominant in more than half of the accepted results. It must be remembered, however, that fine-grained hematite can have unblocking temperatures well below 580 °C, making this component difficult to distinguish from magnetite and titanomagnetite contributions. It is possible that fine-grained hematite is present in all the rocks studied. In fact, the samples with the high hematite concentration indicated by unblocking above 580 °C also show both gradual NRM/susceptibility unblocking below 500 °C and sharp unblocking near the Néel temperature, indicating the presence of hematite with a broad grain size range. This points to the likely growth of hematite through hydrothermal flow during the late stage of the ELIP magmatism (or slightly thereafter). This alteration can be at very low temperatures, and in this case the difference between the temperature of formation and unblocking can be hundreds of °C. Thus, the remanence residing in hematite is probably a very low temperature chemical remanent magnetization (CRM), and/or an intermediate temperature thermochemical remanent magnetization (TCRM) rather than TRM. Such a magnetization can mimic the paleomagnetic field direction of the ELIP rocks, but record an artificially lower strength of the field[34,35]. To summarize, evidence for the lack of averaging of paleosecular variation, MD grains (concave-up shape of Aria plots), and most importantly the presence of hematite and associated CRM or TCRM, cast serious doubt on the reliability of paleointensity results from the Binchuan and Dongchuan lavas.

Supplementary Text 3: Preservation of primary remanent magnetizations in single plagioclase crystals

Our paleomagnetism, rock magnetism, and thermochronology results support a primary origin of NRM in bulk rock of the Baima gabbro. Other evidence suggesting the preservation of a primary NRM in the single plagioclase crystals includes rock magnetism, SEM observations and application of the Néel's SD blocking theory[36] to the thermal history of the Baima gabbro. Rock magnetic analyses and SEM observations indicate that magnetic carriers of the plagioclase crystals are magnetite and titanomagnetite formed during cooling of the magma; no authigenic magnetic mineral is identified (Fig. 3 and Supplementary Figs. 5-8). Application of the Néel's SD blocking theory[36] to the thermal history of the Baima areas[20-22] also suggests that thermal resetting of the NRM recorded by single plagioclase crystals is unlikely (Supplementary Fig. 11). The minimum temperature in the paleointensity fit of most single plagioclase crystals, passing our paleointensity data selection criteria, are above 366 °C. The three grains with minimum temperatures of 296, 332 and 314 °C in their paleointensity fits lost the majority of their NRM above 366 °C (Fig 4, Supplementary Figs. 9, 10, and Supplementary Data 8). The average of the minimum temperatures in paleointensity fit is ~370 °C. The ELIP intrusions in the Baima area cooled to 220 °C by ~258 Ma, 160 °C by ~254 Ma, and 120 °C by ~37 Ma (Fig. 1d). This suggests the rocks were at 220-120 °C for ~221 Myr. In the nomogram of Néel's SD theory[36,37], remanence residing in SD magnetic minerals with relaxation times of ~90 seconds (our laser heating time) that were blocked at 370 °C can be erased if the magnetic carrier is persistently heated to ~220 °C for ~700 Myr, an interval far exceeding the slow cooling duration of ~221 Myr at 220-120 °C. If the temperature remains as low as ~120 °C, the initial remanence can never be removed (Supplementary Fig. 11).

Supplementary Text 4: Paleointensity cooling rate correction

Intrusions in the Baima area cover an area of 12 x 22 km (Supplementary Fig. 1b). Our sampled gabbro is far away from the margin and would have cooled slowly. Slow cooling of the gabbro enhances the recording of the time-averaged geomagnetic field by single plagioclase crystals, resulting in the potential to overestimate paleointensity determined from SD magnetic minerals because of our much faster laboratory cooling rate[38-40]. The size of plagioclase grains in the gabbro discussed here are comparable to these of the Bushveld pyroxenite and Passo da Fabiana gabbro. Therefore, we propose a similar cooling time of ~100 kyr through the unblocking temperature range[41]. Considering an averaged unblocking temperature of ~437 °C (Supplementary Data 8), a cooling rate correction factor of 1.5 was estimated following the approach of Tauxe [42] (Supplementary Fig. 12). This correction factor was subsequently applied to the paleointensity estimates.

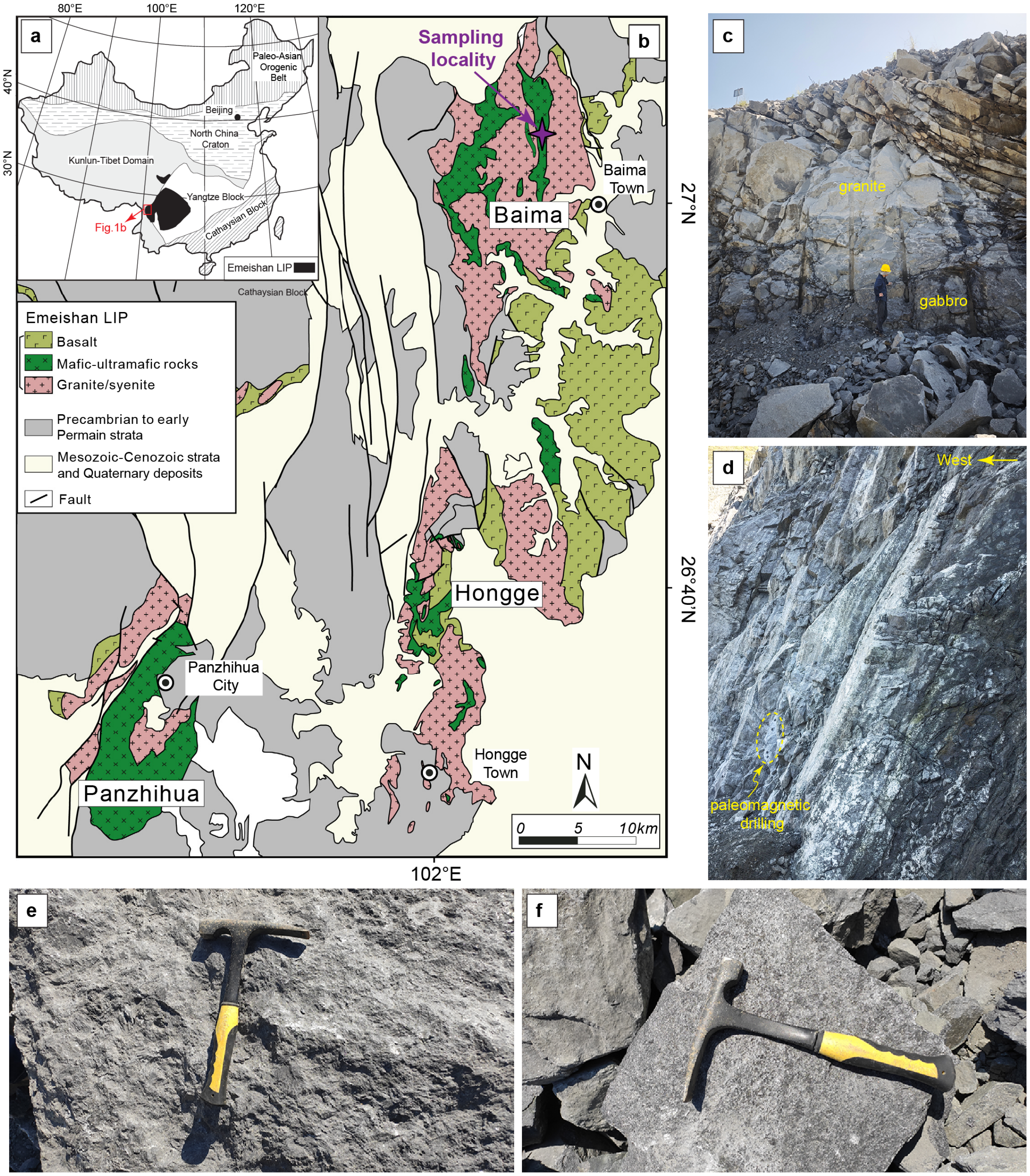

Supplementary Fig. 1 | The Emeishan large igneous province (ELIP) in the Panzhihua region and its exposure near the Baima town. a-b Distribution of the ELIP in the Panzhihua region after Shellnutt[43] and Liu, et al.[18]. **c** Granite and gabbro sampled for geochronology. Gradual transition from granite to gabbro indicates coeval emplacement. **d** Layered gabbro collected for paleomagnetism. Rhythmic layering of dark/light minerals suggests that the gabbro dips to the west with a mean strike/dip of 182°/68° (right-hand-rule). **e-f** Fresh and coarse gabbro collected for single crystal paleointensity.

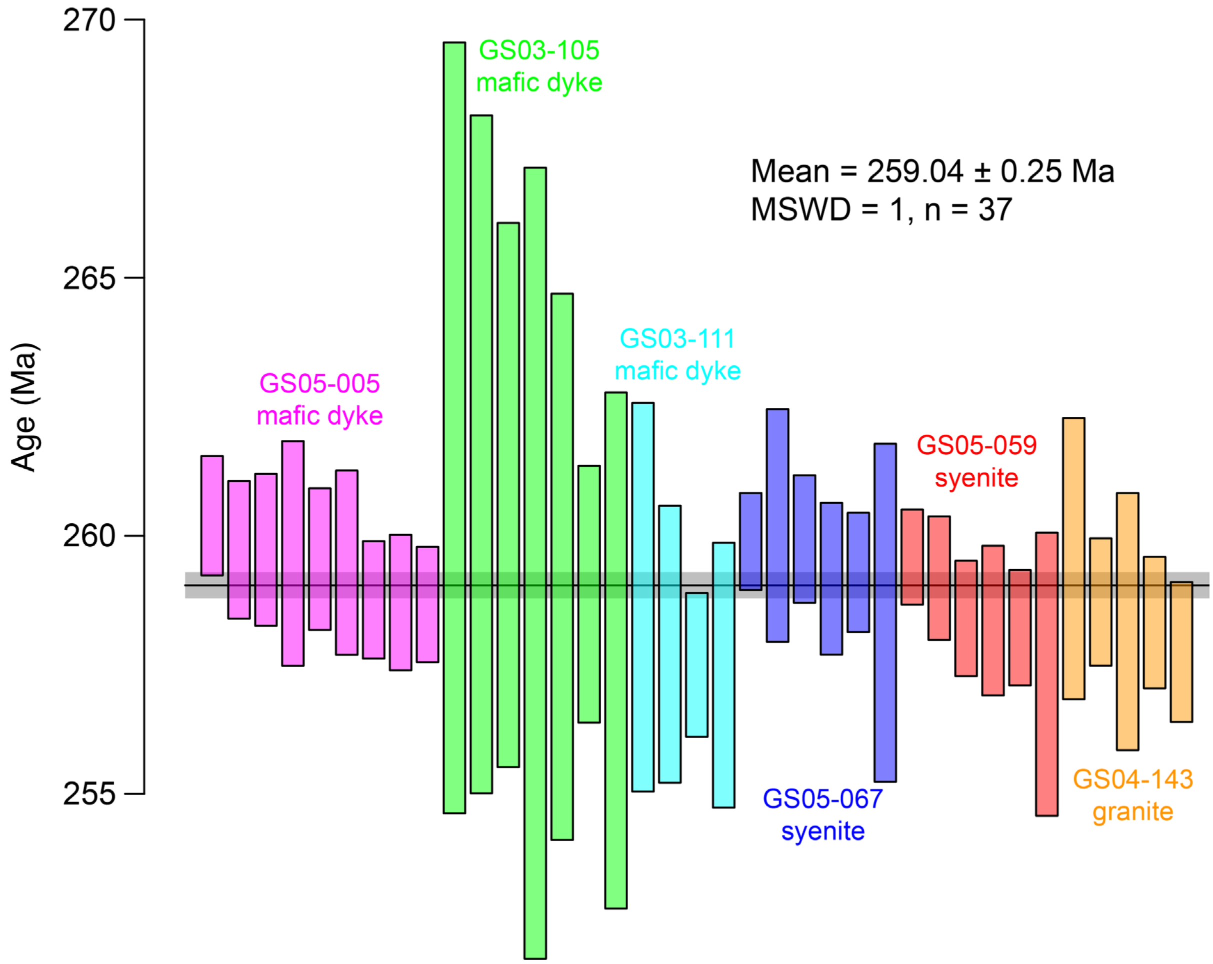

Supplementary Fig. 2 | Single-grain and weighted mean zircon U-Pb chemical-abrasion thermal ionization mass spectrometry dates of six mafic dyke, syenite, granite intrusive samples from the Emeishan large igneous province in the Baima area. Original data are reported by Shellnutt, et al.[8]. MSWD - mean square weighted deviation.

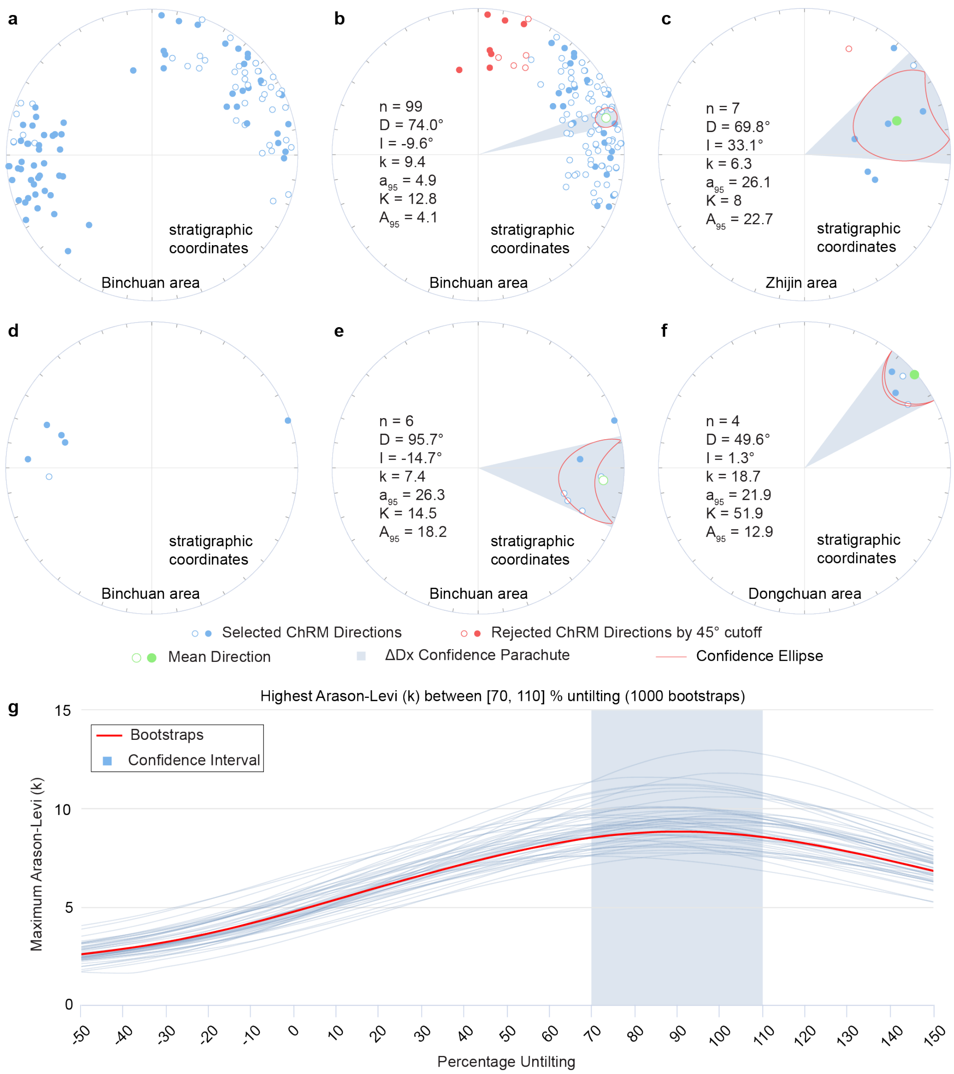

Supplementary Fig. 3 | Equal-area projections of the site-mean characteristic remanent magnetizations (ChRMs) from basaltic lava flows of the Emeishan large igneous province in the Binchuan[11], Zhijin[26] and Dongchuan[33] areas, and a regional inclination only fold test. **a-b** The Binchuan results reported by Xu, et al.[11]. ChRM directions with reversed polarity in **a** were converted to normal polarity for the statistics in **b**. A fixed 45° cutoff based on angular distance of virtual geomagnetic poles from the mean pole was applied. **c** The Zhijin results reported by Thomas, et al.[26]. These authors used the same lavas for bulk rock paleointensity. **d-e** The Binchuan results reported by Zhang, et al.[33] for bulk rock paleointensity. Polarity conversion was applied. **f** The Dongchuan results reported by Zhang, et al.[33] for bulk rock paleointensity. **g** Bootstrapped inclination-only fold test[44,45] applied to ChRMs of the layered gabbro near Baima (this study) and Panzhihua[30], and basaltic lavas in the Binchuan area[11]. The confidence ellipses in equal-area projections are based on A_{95} pole Fisher statistics.

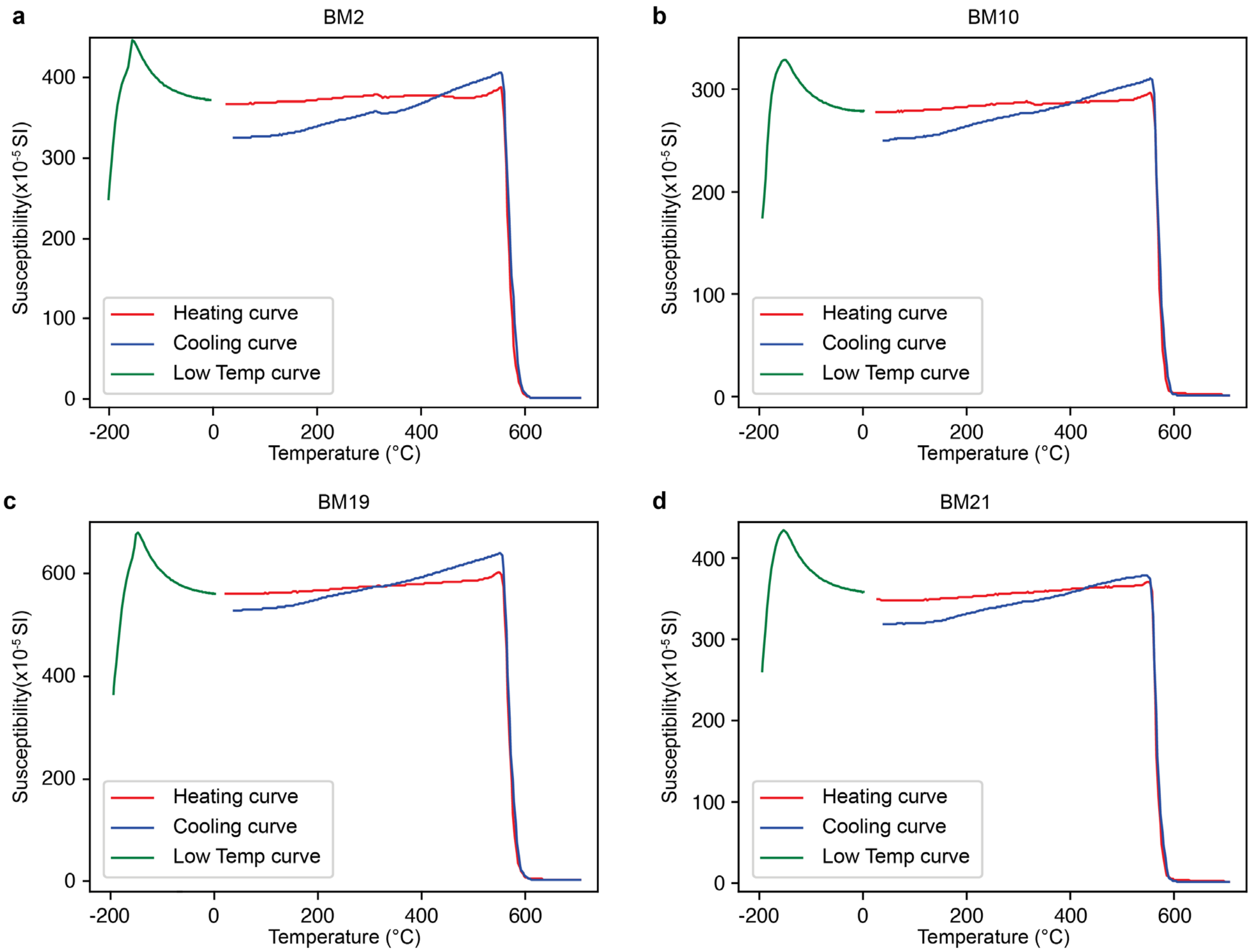

Supplementary Fig. 4 | Magnetic susceptibility versus temperature curves of gabbro samples from the Emeishan large igneous province near the Baima town. All samples were heated and cooled in air.

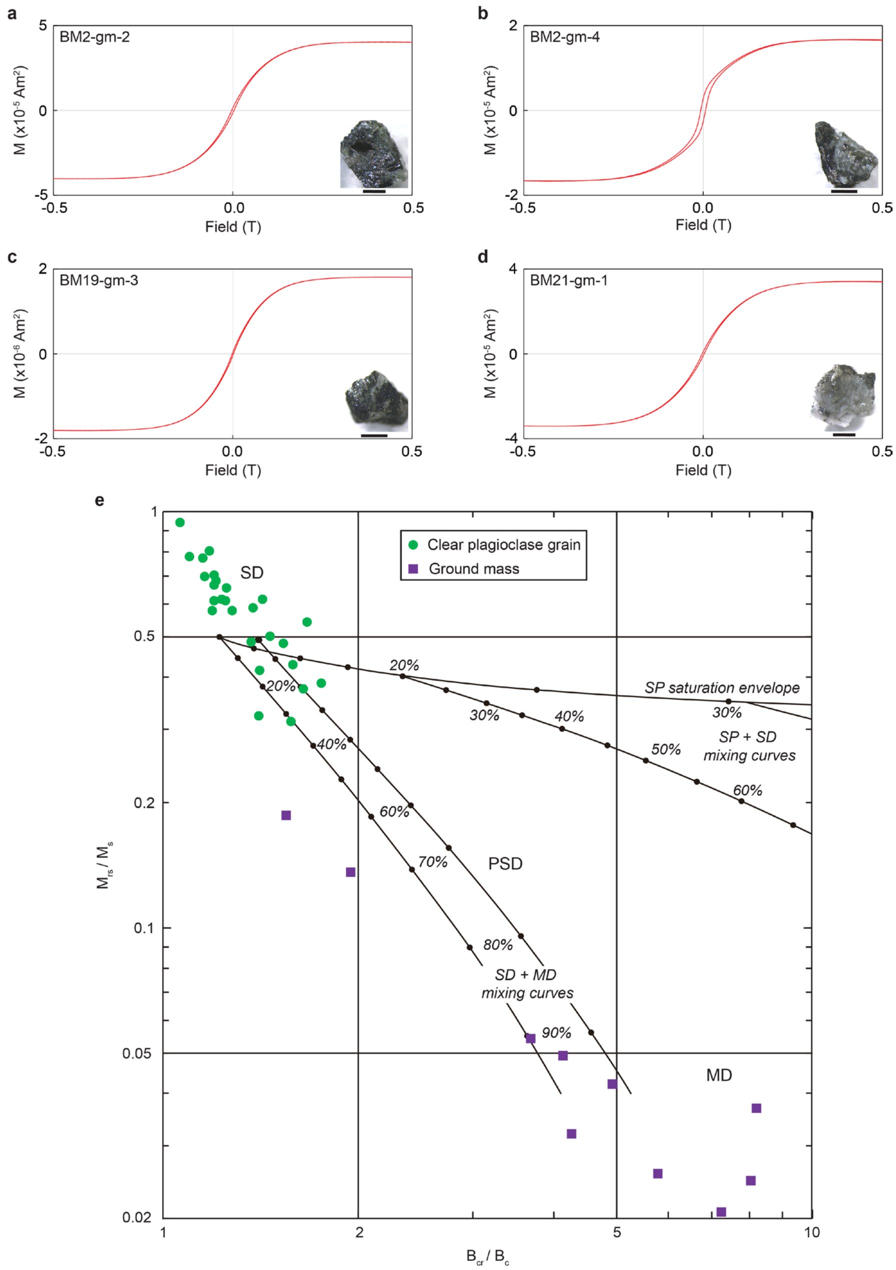

Supplementary Fig. 5 | Magnetic hysteresis loops of the groundmass specimens and Day plot of the clear plagioclase versus groundmass specimens. a-d Magnetic hysteresis loops with images of the measured groundmass specimens from gabbro samples of the Emeishan large igneous province. Scale bar is 1 mm. **e** Day plot of the ratio of hysteresis parameters for groundmass and clear plagioclase crystal specimens[46,47]. Hysteresis parameters are shown in Supplementary Data 3. M_{rs}, remanent saturation; M_s, saturation magnetization; B_c, coercive force; B_{cr}, remanent coercivity; MD, multidomain; PSD, pseudosingle domain; SD, single domain; SP, superparamagnetic.

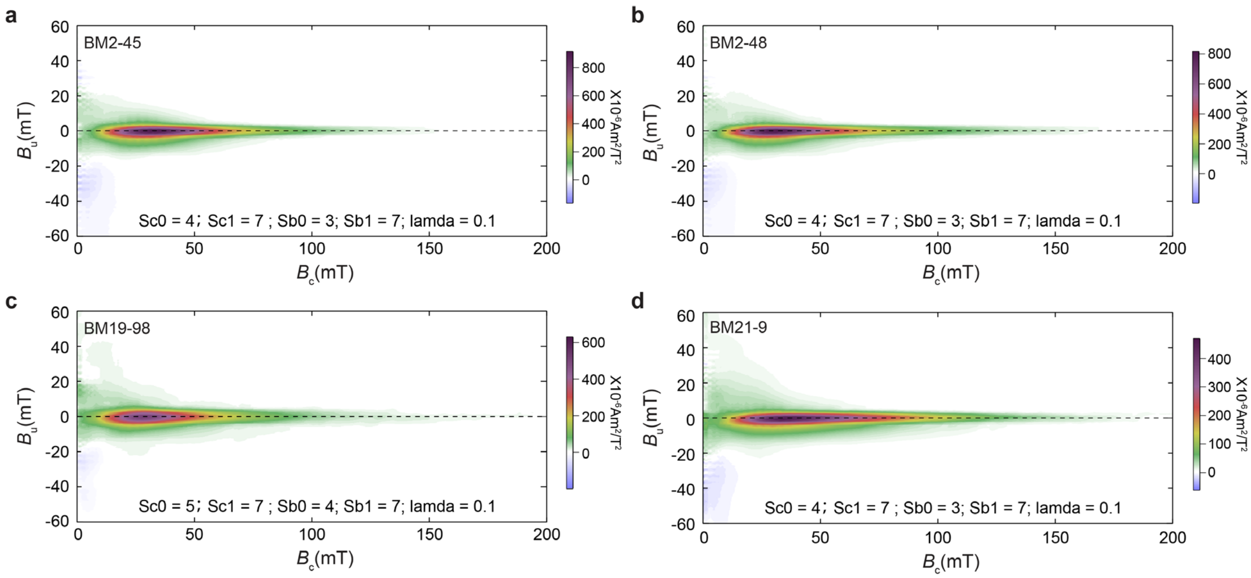

Supplementary Fig. 6 | Additional first-order reversal curve (FORC) diagrams of the clear plagioclase crystal specimens. FORC smoothing parameters (Sc0, Sc1, Sb0, Sb1, and lamda) are also shown for each specimen.

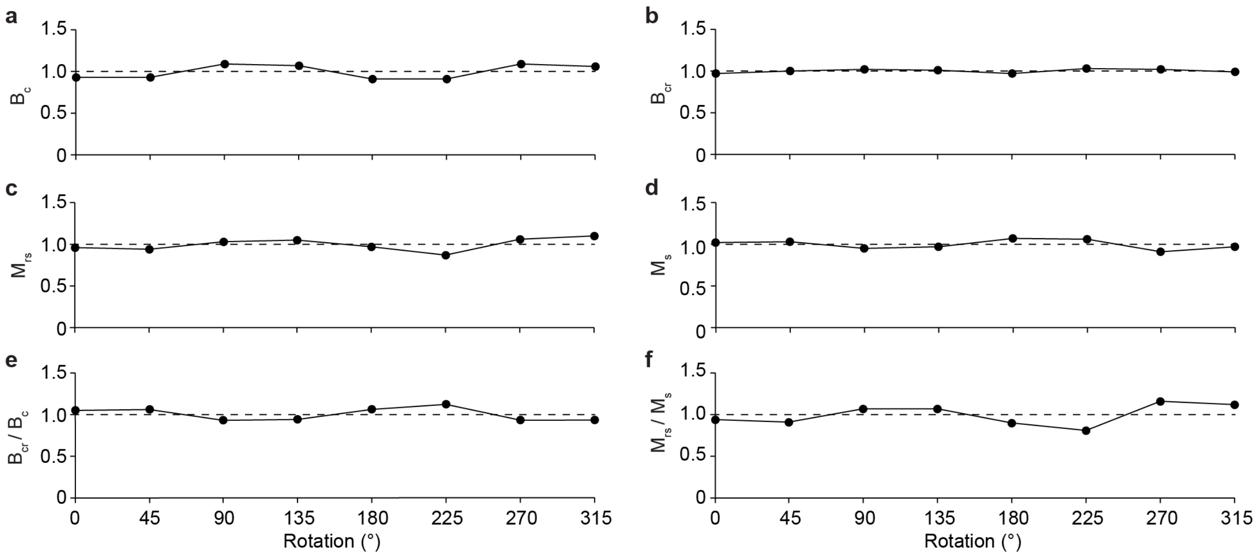

Supplementary Fig. 7 | Hysteresis parameters normalized by the mean values versus rotation angle for a clear plagioclase crystal. The crystal was rotated by 45° steps. Hysteresis parameters are shown in Supplementary Data 4. M_{rs}, remanent saturation; M_s, saturation magnetization; B_c, coercive force; B_{cr}, remanent coercivity.

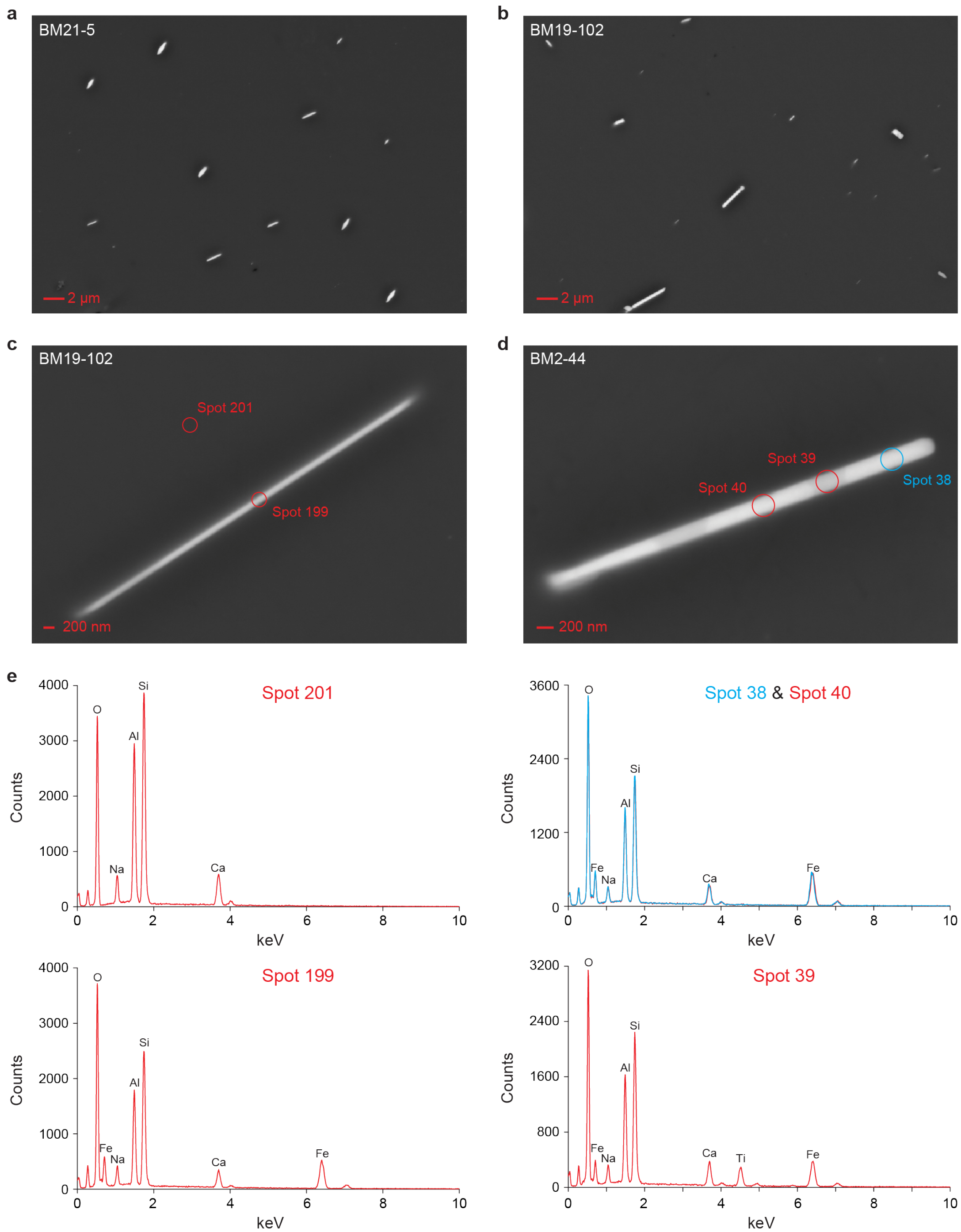

Supplementary Fig. 8 | Additional scanning electron microscopy (SEM) images and associated energy-dispersive spectroscopy (EDS) analyses of Fe-Ti oxide needles in plagioclase crystals from gabbro samples of the Emeishan large igneous province. a-d SEM backscatter images of the plagioclase crystals with the spots of EDS analysis. **e** EDS results of the plagioclase background (Spot 201) and Fe-Ti oxide needles (Spots 38, 39, 40, and 199) in **c** and **d**. Fe and Ti contents are presented in Supplementary Data 7.

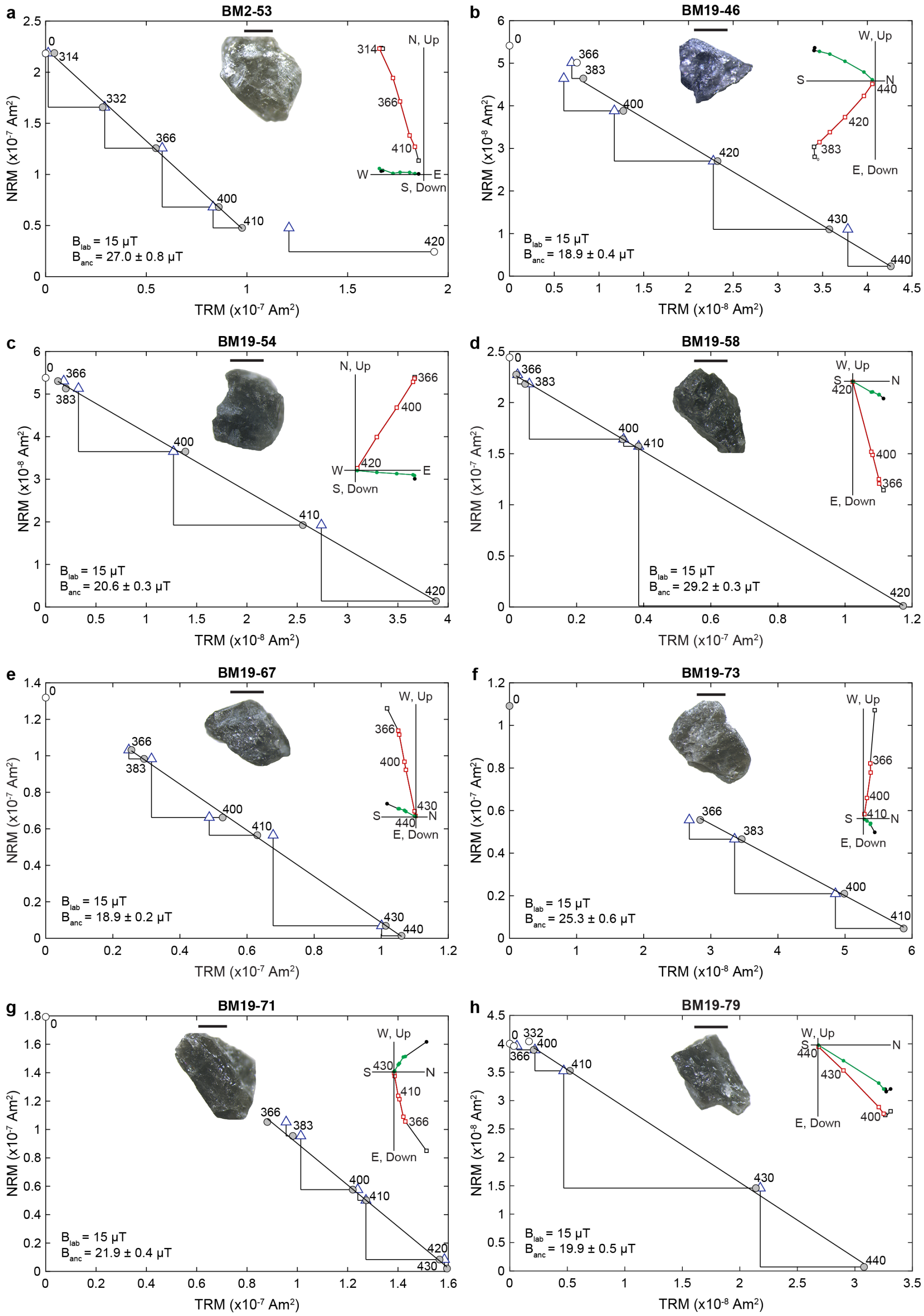

Supplementary Fig. 9 | Additional Thellier-Coe paleointensity measurement on single plagioclase crystals from gabbro samples of the Emeishan large igneous province with an applied lab field of 15 μT. See caption of Fig. 5 in the main text for an explanation of symbols. All results are category A. NRM, natural remanent magnetization; TRM, thermal remanent magnetization.

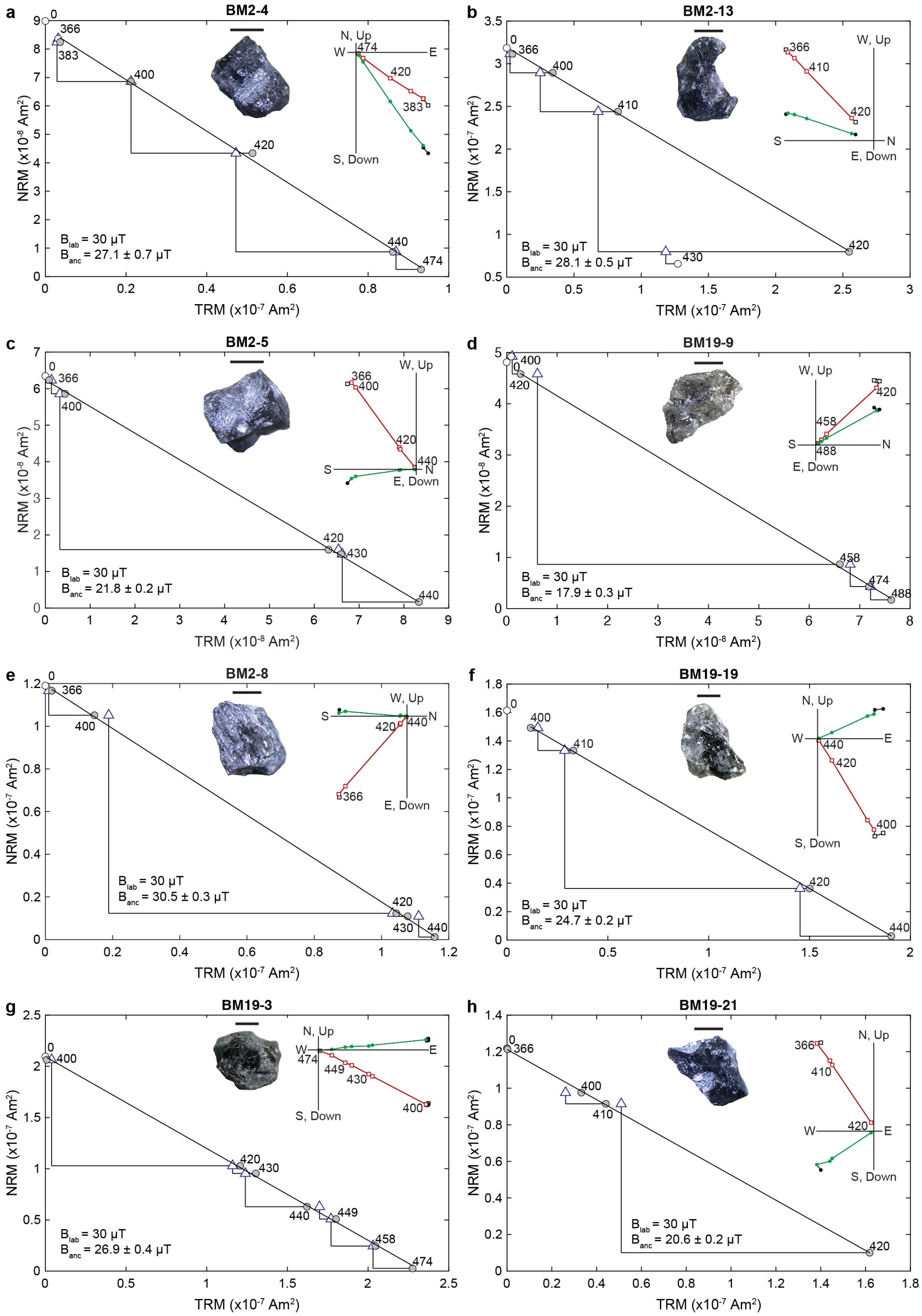

Supplementary Fig. 10 | Additional Thellier-Coe paleointensity measurement on single plagioclase crystals with an applied lab field of 30 μT. See caption of Fig. 5 in the main text for an explanation of symbols. Result of specimen BM19-21 is category B, others are category A. NRM, natural remanent magnetization; TRM, thermal remanent magnetization.

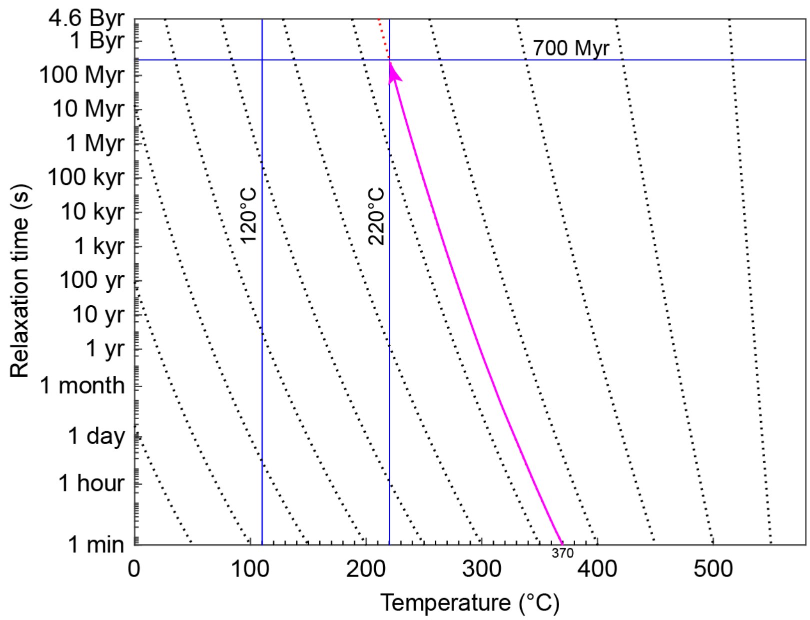

Supplementary Fig. 11 | Plot of remanence unblocking at 370 °C in lab heating and its fate on nomograms of Néel's single domain theory[36], modified after Pullaiah, et al.[48] and Berndt and Chang[37]. Slow cooling of the gabbro from 220 to 120 °C (time-temperature history in Fig. 1d) after emplacement must last >700 Myr to billions of years in order to reset the remanence carried by the ELIP plagioclase, far exceeding the cooling duration of ~221 Myr (258-37 Ma) at these relatively low temperatures. Recent micromagnetic simulations indicate that magnetocrystalline anisotropy may modify relaxation times relative to those predicted by the classical Néel-Pullaiah framework[49,50]. Accordingly, the calculations presented here should be regarded as a first-order estimate of remanence stability.

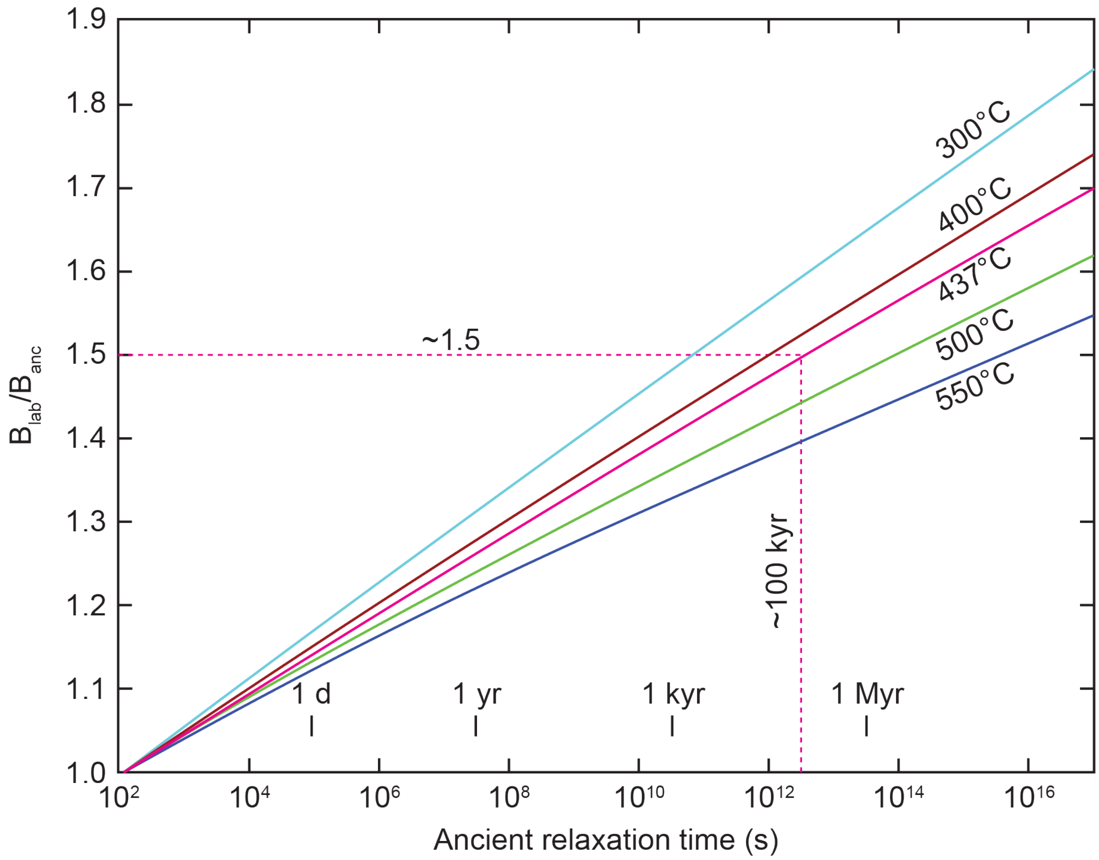

Supplementary Fig. 12 | Ratio of laboratory field intensity (B_{lab}) to ancient field intensity (B_{anc}) as a function of cooling time at different blocking temperatures, calculated following the model of Tauxe[42]. Plagioclase crystals in gabbro from the Emeishan large igneous province (ELIP) have a mean unblocking temperature of ~437 °C (Supplementary Data 8). Based on the comparable grain sizes of the ELIP, Bushveld, and Passo da Fabiana intrusions[41], we infer a cooling time of ~100 kyr through the unblocking temperature interval, corresponding to a cooling rate correction factor of 1.5.

References

1 Song, X.-Y. *et al.* Geochemical constraints on the mantle source of the upper Permian Emeishan continental flood basalts, southwestern China. *International Geology Review* **43**, 213-225 (2001).

2 Xu, Y.-G. *et al.* Zircon U–Pb and Hf isotope constraints on crustal melting associated with the Emeishan mantle plume. *Geochimica et Cosmochimica Acta* **72**, 3084-3104 (2008). https://doi.org/https://doi.org/10.1016/j.gca.2008.04.019

3 Xu, Y., Chung, S.-L., Jahn, B.-m. & Wu, G. Petrologic and geochemical constraints on the petrogenesis of Permian–Triassic Emeishan flood basalts in southwestern China. *Lithos* **58**, 145-168 (2001).

4 Zhou, M.-F. *et al.* Geochemistry, Petrogenesis and Metallogenesis of the Panzhihua Gabbroic Layered Intrusion and Associated Fe–Ti–V Oxide Deposits, Sichuan Province, SW China. *Journal of Petrology* **46**, 2253-2280 (2005). https://doi.org/10.1093/petrology/egi054

5 He, B. *et al.* Age and duration of the Emeishan flood volcanism, SW China: geochemistry and SHRIMP zircon U–Pb dating of silicic ignimbrites, post-volcanic Xuanwei Formation and clay tuff at the Chaotian section. *Earth and Planetary Science Letters* **255**, 306-323 (2007).

6 He, B., Xu, Y.-G., Zhong, Y.-T. & Guan, J.-P. The Guadalupian–Lopingian boundary mudstones at Chaotian (SW China) are clastic rocks rather than acidic tuffs: implication for a temporal coincidence between the end-Guadalupian mass extinction and the Emeishan volcanism. *Lithos* **119**, 10-19 (2010).

7 Sun, Y. *et al.* Dating the onset and nature of the Middle Permian Emeishan large igneous province eruptions in SW China using conodont biostratigraphy and its bearing on mantle plume uplift models. *Lithos* **119**, 20-33 (2010).

8 Shellnutt, J. G., Denyszyn, S. W. & Mundil, R. Precise age determination of mafic and felsic intrusive rocks from the Permian Emeishan large igneous province (SW China). *Gondwana Research* **22**, 118-126 (2012).

9 Zhong, Y.-T., He, B., Mundil, R. & Xu, Y.-G. CA-TIMS zircon U–Pb dating of felsic ignimbrite from the Binchuan section: Implications for the termination age of Emeishan large igneous province. *Lithos* **204**, 14-19 (2014).

10 Huang, H. *et al.* Eruptive tempo of Emeishan large igneous province, southwestern China and northern Vietnam: Relations to biotic crises and paleoclimate changes around the Guadalupian-Lopingian boundary. *Geology* **50**, 1083-1087 (2022).

11 Xu, Y. *et al.* Rapid eruption of the Emeishan continental flood basalts: New paleomagnetic and geochronologic constraints. *GSA Bulletin* **134**, 1845-1862 (2022).

12 Huang, K. & Opdyke, N. D. Magnetostratigraphic investigations on an Emeishan basalt section in western Guizhou province, China. *Earth and Planetary Science Letters* **163**, 1-14 (1998).

13 Ali, J. R., Thompson, G. M., Song, X. & Wang, Y. Emeishan basalts (SW China) and the 'end-Guadalupian'crisis: magnetobiostratigraphic constraints. *Journal of the Geological Society* **159**, 21-29 (2002).

14 Li, Y. *et al.* 40Ar/39Ar age of the onset of high-Ti phase of the Emeishan volcanism strengthens the link with the end-Guadalupian mass extinction. *International Geology Review* **60**, 1906-1917 (2018).

15 Fan, W. Ar-Ar and U-Pb geochronol-ogy of Late Paleozoic basalts in western Guangxi and its constraints on the eruption age of Emeishan basalt mag-matism. *Chinese Science Bulletin* **49**, 2318 (2004).
16 Lo, C.-H., Chung, S.-L., Lee, T.-Y. & Wu, G. Age of the Emeishan flood magmatism and relations to Permian–Triassic boundary events. *Earth and Planetary Science Letters* **198**, 449-458 (2002).
17 Ali, J. R., Lo, C.-H., Thompson, G. M. & Song, X. Emeishan Basalt Ar-Ar overprint ages define several tectonic events that affected the western Yangtze platform in the Mesozoic and Cenozoic. *Journal of Asian Earth Sciences* **23**, 163-178 (2004).
18 Liu, P.-P., Zhou, M.-F., Ren, Z., Wang, C. Y. & Wang, K. Immiscible Fe-and Si-rich silicate melts in plagioclase from the Baima mafic intrusion (SW China): implications for the origin of bi-modal igneous suites in large igneous provinces. *Journal of Asian Earth Sciences* **127**, 211-230 (2016).
19 Zhang, X.-Q. *et al.* Fractional crystallization and the formation of thick Fe-Ti-V oxide layers in the Baima layered intrusion, SW China. *Ore Geology Reviews* **49**, 96-108 (2012).
20 Zhang, G. *et al.* Progressive tectonic evolution from crustal shortening to mid-lower crustal expansion in the southeast Tibetan Plateau: A synthesis of structural and thermochronological insights. *Earth-Science Reviews*, 103951 (2022).
21 Zhang, Y., Yan, D.-P., Qiu, L., Gong, L. & Shao, Y. Stepwise growth of the southeastern Tibetan Plateau: Structural and thermochronological evidence from the Panxi tectonic belt. *Palaeogeography, Palaeoclimatology, Palaeoecology* **621**, 111542 (2023).
22 Hu, D. *et al.* Thermal imprints of late Permian Emeishan basalt effusion: Evidence from zircon fission-track thermochronology. *Lithos* **352-353**, 105224 (2020). https://doi.org/https://doi.org/10.1016/j.lithos.2019.105224
23 Zhao, X. & Coe, R. S. Palaeomagnetic constraints on the collision and rotation of North and South China. *Nature* **327**, 141-144 (1987).
24 McElhinny, M., Embleton, B., Ma, X. & Zhang, Z. Fragmentation of Asia in the Permian. *Nature* **293**, 212-216 (1981).
25 Van der Voo, R. *et al.* Paleomagnetism and electron microscopy of the Emeishan basalts, Yunnan, China. *Tectonophysics* **221**, 367-379 (1993).
26 Thomas, D., Rolph, T., Shaw, J., Gonzalez de Sherwood, S. & Zhuang, Z. Palaeointensity studies of a late Permian lava succession from Guizhou Province, South China: implications for post-Kiaman dipole field behaviour. *Geophysical Journal International* **134**, 856-866 (1998).
27 Liu, C. & Zhu, R. Geodynamic significances of the Emeishan Basalts. *Earth Science Frontiers* **16**, 52-69 (2009).
28 Zheng, L., Yang, Z., Tong, Y. & Yuan, W. Magnetostratigraphic constraints on two-stage eruptions of the Emeishan continental flood basalts. *Geochemistry, Geophysics, Geosystems* **11** (2010).
29 Xu, Y., Yang, Z., Tong, Y. B. & Jing, X. Paleomagnetic secular variation constraints on the rapid eruption of the Emeishan continental flood basalts in southwestern China and northern Vietnam. *Journal of Geophysical Research: Solid Earth* **123**, 2597-2617 (2018).
30 Krivolutskaya, N. *et al.* Correlation of intrusive and volcanic rocks in Emeishan Large Igneous Province by geochemical and paleomagnetic data. *Proceedings of the 11th Intl School and Conference "Problems of Geocosmos"*, 45-53 (2016).

31 Liu, C., Paterson, G. A., Li, S., Pan, Y. & Zhu, R. Remagnetization of Permian Emeishan basalts: Constraints on the timing of native copper mineralization in northeast Yunnan Province, China. *Frontiers in Earth Science* **8** (2021).
32 Zhu, R., Liu, C. & Pan, Y. in *AGU Fall Meeting Abstracts.* GP31A-1098 (2011).
33 Zhang, W. *et al.* Extremely weak geomagnetic field following Permo-Carboniferous reverse superchron and its geological implications. *Geophysical Research Letters* **52**, e2025GL115474 (2025).
34 Smirnov, A. & Tarduno, J. Thermochemical remanent magnetization in Precambrian rocks: Are we sure the geomagnetic field was weak? *Journal of Geophysical Research: Solid Earth* **110** (2005).
35 Huang, W., Cottrell, R. D. & Tarduno, J. A. No evidence for extreme high fields or inner core nucleation 1.1 billion years ago from the Midcontinent Rift of North America. *Geophysical Journal International* **243**, ggaf343 (2025).
36 Néel, L. Théorie du traînage magnétique des ferromagnétiques en grains fins avec applications aux terres cuites. *Ann. géophys* **5**, 99-136 (1949).
37 Berndt, T. A. & Chang, L. Theory of stable multi-domain thermoviscous remanence based on repeated domain-wall jumps. *Journal of Geophysical Research: Solid Earth* **123**, 10399-10417, doi: 10310.11029/12018JB016816 (2019).
38 Yu, Y. Importance of cooling rate dependence of thermoremanence in paleointensity determination. *Journal of Geophysical Research: Solid Earth* **116** (2011).
39 Nagy, L., Williams, W. & Tauxe, L. Estimating the effect of cooling rate on the acquisition of magnetic remanence. *Geophysical Research Letters* **48**, e2021GL095284 (2021).
40 Halgedahl, S., Day, R. & Fuller, M. The effect of cooling rate on the intensity of weak-field TRM in single-domain magnetite. *Journal of Geophysical Research: Solid Earth* **85**, 3690-3698 (1980).
41 Huang, W. *et al.* Near-collapse of the geomagnetic field may have contributed to atmospheric oxygenation and animal radiation in the Ediacaran Period. *Communications Earth & Environment* **5**, 207 (2024). https://doi.org/10.1038/s43247-024-01360-4
42 Tauxe, L. (ed University of California Press) (2010).
43 Shellnutt, J. G. The Emeishan large igneous province: A synthesis. *Geoscience Frontiers* **5**, 369-394 (2014).
44 Enkin, R. J. & Watson, G. S. Statistical analysis of palaeomagnetic inclination data. *Geophysical Journal International* **126**, 495-504 (1996).
45 Arason, Þ. & Levi, S. Maximum likelihood solution for inclination-only data in paleomagnetism. *Geophysical Journal International* **182**, 753-771 (2010).
46 Day, R., Fuller, M. & Schmidt, V. Hysteresis properties of titanomagnetites: grain-size and compositional dependence. *Physics of the Earth and Planetary Interiors* **13**, 260-267 (1977).
47 Dunlop, D. J. Theory and application of the Day plot (M_{rs}/M_s versus H_{cr}/H_c) 1. Theoretical curves and tests using titanomagnetite data. *Journal of Geophysical Research: Solid Earth* **107**, 2056, doi: 2010.1029/2001JB000486 (2002).
48 Pullaiah, G., Irving, E., Buchan, K. L. & Dunlop, D. J. Magnetization changes caused by burial and uplift. *Earth and Planetary Science Letters* **28**, 133-143 (1975).

49 Cych, B., Paterson, G. A., Nagy, L. & Williams, W. First principles understanding of single domain magnetizations—Part I: the single domain comprehensive calculator (SDCC) open source library. *Geophysical Journal International* **241**, 2033-2047 (2025).
50 Cych, B., Paterson, G. A., Nagy, L., Williams, W. & Tauxe, L. First principles understanding of single domain magnetizations—Part II: Non-ideal magnetic behaviour in ideal single domain titanomagnetite. *Geophysical Journal International* **245**, ggag090 (2026).
51 Heslop, D. & Roberts, A. P. Analyzing paleomagnetic data: to anchor or not to anchor? *Journal of Geophysical Research: Solid Earth* (2016).